



Development of Sulfide Solid Electrolytes and Interface Formation Processes for Bulk-Type All-Solid-State Li and Na Batteries

Akitoshi Hayashi^{1*}, Atsushi Sakuda^{1,2} and Masahiro Tatsumisago¹

¹ Department of Applied Chemistry, Graduate School of Engineering, Osaka Prefecture University, Sakai, Osaka, Japan,

² Department of Energy and Environment, Research Institute of Electrochemical Energy, National Institute of Advanced Industrial Science and Technology (AIST), Ikeda, Osaka, Japan

OPEN ACCESS

Edited by:

Shyue Ping Ong,
University of California,
San Diego, USA

Reviewed by:

Liqiang Mai,
Wuhan University of
Technology, China
Xiao-Liang Wang,
Seeo Inc., USA

*Correspondence:

Akitoshi Hayashi
hayashi@chem.osakafu-u.ac.jp

Specialty section:

This article was submitted
to Energy Storage,
a section of the journal
Frontiers in Energy Research

Received: 01 March 2016

Accepted: 16 June 2016

Published: 15 July 2016

Citation:

Hayashi A, Sakuda A and
Tatsumisago M (2016) Development
of Sulfide Solid Electrolytes and
Interface Formation Processes
for Bulk-Type All-Solid-State
Li and Na Batteries.
Front. Energy Res. 4:25.
doi: 10.3389/fenrg.2016.00025

All-solid-state batteries with inorganic solid electrolytes (SEs) are recognized as an ultimate goal of rechargeable batteries because of their high safety, versatile geometry, and good cycle life. Compared with thin-film batteries, increasing the reversible capacity of bulk-type all-solid-state batteries using electrode active material particles is difficult because contact areas at solid–solid interfaces between the electrode and electrolyte particles are limited. Sulfide SEs have several advantages of high conductivity, wide electrochemical window, and appropriate mechanical properties, such as formability, processability, and elastic modulus. Sulfide electrolyte with $\text{Li}_7\text{P}_3\text{S}_{11}$ crystal has a high Li^+ ion conductivity of $1.7 \times 10^{-2} \text{ S cm}^{-1}$ at 25°C . It is far beyond the Li^+ ion conductivity of conventional organic liquid electrolytes. The Na^+ ion conductivity of $7.4 \times 10^{-4} \text{ S cm}^{-1}$ is achieved for $\text{Na}_{3.06}\text{P}_{0.94}\text{Si}_{0.06}\text{S}_4$ with cubic structure. Moreover, formation of favorable solid–solid interfaces between electrode and electrolyte is important for realizing solid-state batteries. Sulfide electrolytes have better formability than oxide electrolytes. Consequently, a dense electrolyte separator and closely attached interfaces with active material particles are achieved via “room-temperature sintering” of sulfides merely by cold pressing without heat treatment. Elastic moduli for sulfide electrolytes are smaller than that of oxide electrolytes, and $\text{Na}_2\text{S}-\text{P}_2\text{S}_5$ glass electrolytes have smaller Young’s modulus than $\text{Li}_2\text{S}-\text{P}_2\text{S}_5$ electrolytes. Cross-sectional SEM observations for a positive electrode layer reveal that sulfide electrolyte coating on active material particles increases interface areas even with a minimum volume of electrolyte, indicating that the energy density of bulk-type solid-state batteries is enhanced. Both surface coating of electrode particles and preparation of nanocomposite are effective for increasing the reversible capacity of the batteries. Our approaches to form solid–solid interfaces are demonstrated.

Keywords: all-solid-state battery, lithium battery, sodium battery, sulfide, solid electrolyte, electrode–electrolyte interface

INTRODUCTION

All-solid-state batteries using inorganic solid electrolytes (SEs), used in place of conventional organic liquid electrolytes, have been studied because of their high safety (non-flammability with no liquid leakage), long cycle life, and versatile geometries (Takada, 2013; Tatsumisago et al., 2013; Tatsumisago and Hayashi, 2014). These features are important for large rechargeable lithium batteries with high energy density for application to eco-cars, such as electric vehicles and plug-in hybrid vehicles. Rechargeable sodium batteries are also attractive for large-scale applications for stationary load-leveling because sodium is expected to be the next targeted element after lithium based on its atomic weight, standard potential, and natural abundance (Yabuchi et al., 2015b; Yamada, 2014).

A key material to realize all-solid-state rechargeable batteries is a superior SE. In lithium ion conductors, sulfide electrolytes of $\text{Li}_{10}\text{GeP}_2\text{S}_{12}$ and $\text{Li}_7\text{P}_3\text{S}_{11}$ have high room-temperature conductivity of more than $10^{-2} \text{ S cm}^{-1}$, which is as high as the conductivity of conventional organic liquid electrolytes (Kamaya et al., 2011; Seino et al., 2014). The lithium ion transport number of liquid electrolytes is below 0.5, whereas that of SE is 1. It is noteworthy that the conductivity of lithium ions of sulfide SEs already exceeds that of organic liquid electrolytes. Very recently, $\text{Li}_{9.54}\text{Si}_{1.74}\text{P}_{1.44}\text{S}_{11.7}\text{Cl}_{0.3}$ has been reported to show the highest conductivity of $2.5 \times 10^{-2} \text{ S cm}^{-1}$. Using this superior electrolyte, high power competing with that of supercapacitors can be achieved in all-solid-state rechargeable lithium batteries (Kato et al., 2016b). Sulfide SEs have several important benefits of high conductivity, wide electrochemical window, and appropriate mechanical properties, such as formability and elastic modulus. A shortcoming of sulfide electrolytes is its low air stability. To realize bulk-type all-solid-state batteries, the formation of favorable solid–solid interfaces between electrode and electrolyte is important in addition to the development of superior sulfide electrolytes. Direct coating of sulfide electrolytes on active material particles instead of adding electrolyte particle is effective for forming a close solid–solid interface with large contact area. Insulative active materials, such as sulfur and Li_2S , should be blended not only with SE but also with carbon-conductive additive to form ion and electron conduction paths to active materials. Nanocomposites of the three components are useful by preparation with high-energy ball milling, which pulverizes and combines them. Transition metal sulfides (MS_x) with high conductivity have good compatibility with sulfide SEs having the same sulfide anions. Especially, sulfur-rich compounds, such as TiS_3 , are attractive active materials with high reversible capacity. Lithium metal is a supremely negative electrode, but issues related to lithium dendrites prevent its commercialization. Combination with a SE is a promising solution. Interface modification between Li metal and the SE is important.

As described in this paper, the recent development of sulfide SEs and interface formation processes for bulk-type all-solid-state Li and Na batteries are reviewed. Significant properties as SEs of conductivity, chemical stability, and mechanical property for Li^+ or Na^+ ion conducting sulfides are reported. Procedures for preparing sulfide electrolytes, such as mechanical milling and liquid-phase synthesis, are also described. Several approaches to form

favorable solid–solid interfaces developed by our research group are demonstrated. Processes for the coating of sulfide electrolytes *via* gas-phase or liquid-phase process on LiCoO_2 or graphite particles have been developed. Preparation of nanocomposite electrodes with sulfur, Li_2S , and Li_3PS_4 (as a bifunctional material of electrolyte and electrode) particles is described, along with the use of MS_x active materials. Formation of a solid–solid interface for using lithium metal negative electrodes is also discussed.

DEVELOPMENT OF SULFIDE SOLID ELECTROLYTES

Sulfide SEs with Li^+ or Na^+ ion conductivity have been developed during the past three decades. Recently, chemical stability and mechanical properties as well as conductivity for sulfide electrolytes have attracted much attention. Sulfide electrolytes are prepared using several techniques with solid-phase reaction, melt-quenching, mechanical milling, crystallization of mother glasses, and liquid-phase reaction. Detailed information related to electrolyte properties will be presented in the following sections of this report.

Conductivity

Inorganic sulfide SEs with high Li^+ or Na^+ ion conductivities have been developed. Sulfide electrolytes with high conductivities are presented in **Table 1**. In Li^+ ion conducting sulfide electrolytes, crystalline $\text{Li}_{10}\text{GeP}_2\text{S}_{12}$ (LGPS; Kamaya et al., 2011) and glass–ceramic $\text{Li}_7\text{P}_3\text{S}_{11}$ (Seino et al., 2014) have considerably high conductivity of more than $10^{-2} \text{ S cm}^{-1}$ at 25°C , which is beyond the Li^+ ion conductivity of conventional organic liquid electrolytes. Very recently, $\text{Li}_{9.54}\text{Si}_{1.74}\text{P}_{1.44}\text{S}_{11.7}\text{Cl}_{0.3}$ with LGPS structure has been reported to show the highest conductivity of $2.5 \times 10^{-2} \text{ S cm}^{-1}$ (Kato et al., 2016b). Studies investigating new electrolytes with much higher conductivity are in progress. Several crystals, such as $\text{Li}_{10}\text{SnP}_2\text{S}_{12}$ (Boron et al., 2013) and $\text{Li}_6\text{PS}_5\text{Cl}$ (Boulineau et al., 2012), have high conductivity of more than $10^{-3} \text{ S cm}^{-1}$. This conductivity is also achieved by the addition of lithium halides to sulfide glass and glass–ceramic electrolytes (Wada et al., 1983; Ujiie et al., 2014).

The Na^+ ion conductivity is lower than Li^+ ion conductivity in glassy electrolytes. Ionic conduction of Na^+ ion with ionic radius larger than Li^+ ion is unfavorable in glasses (Souquet et al., 1981). For sodium ion conductors, sulfides with high conductivity had not been found since this report described Na_3PS_4 glass–ceramic electrolytes in 2012. A cubic Na_3PS_4 phase is precipitated by crystallization of a mother Na_3PS_4 glass. The prepared glass–ceramic electrolyte shows Na^+ ion conductivity of greater than $10^{-4} \text{ S cm}^{-1}$ at 25°C (Hayashi et al., 2012b). Furthermore, partial substitution of Si for P in Na_3PS_4 is useful for increasing conductivity (Tanibata et al., 2014). **Figure 1** presents the composition dependence of conductivities at 25°C for Na_3PS_4 – Na_4Si_4 glass–ceramic electrolytes. The replacement of 6 mol% Na_3PS_4 by Na_4Si_4 increases the conductivity from 4.6×10^{-4} to $7.4 \times 10^{-4} \text{ S cm}^{-1}$. The electron density distribution of the cubic Na_3PS_4 structure obtained using the maximum entropy method is shown in the inset of **Figure 1**. Na_3PS_4 has three-dimensional

TABLE 1 | Li⁺ ion and Na⁺ ion conductivities for sulfide solid electrolytes.

Composition	Conductivity at 25°C (S cm ⁻¹)	Classification	Reference
Li _{9.54} Si _{1.74} P _{1.44} S _{11.7} Cl _{0.3}	2.5 × 10 ⁻²	Crystal	(Kato et al. 2016b)
Li ₁₀ GeP ₂ S ₁₂	1.2 × 10 ⁻²	Crystal	Kamaya et al. (2011)
Li ₁₀ SnP ₂ S ₁₂	4 × 10 ⁻³	Crystal	Boron et al. (2013)
Li _{3.833} Sn _{0.833} As _{0.166} S ₄	1.4 × 10 ⁻³	Crystal	Sahu et al. (2014)
Li ₆ PS ₅ Cl	1.3 × 10 ⁻³	Crystal	Boulineau et al. (2012)
70Li ₂ S·30P ₂ S ₅ (Li ₇ P ₃ S ₁₁)	1.7 × 10 ⁻²	Glass–ceramic	Seino et al. (2014)
63Li ₂ S·27P ₂ S ₅ ·10LiBr	8.4 × 10 ⁻³	Glass–ceramic	Ujiiie et al. (2014)
80Li ₂ S·20P ₂ S ₅	1.3 × 10 ⁻³	Glass–ceramic	Mizuno et al. (2006)
30Li ₂ S·26B ₂ S ₃ ·44LiI	1.7 × 10 ⁻³	Glass	Wada et al. (1983)
50Li ₂ S·17P ₂ S ₅ ·33LiBH ₄	1.6 × 10 ⁻³	Glass	Yamauchi et al. (2013)
63Li ₂ S·36SiS ₂ ·1Li ₃ PO ₄	1.5 × 10 ⁻³	Glass	Aotani et al. (1994)
70Li ₂ S·30P ₂ S ₅	1.6 × 10 ⁻⁴	Glass	Zhang and Kennedy (1990)
Na ₃ PSe ₄	1.2 × 10 ⁻³	Crystal	Zhang et al. (2015)
Na ₃ PS ₄ (tetragonal)	1 × 10 ⁻⁶	Crystal	Jansen and Henseler (1992)
94Na ₃ PS ₄ ·6Na ₄ SiS ₄	7.4 × 10 ⁻⁴	Glass–ceramic	Tanibata et al. (2014)
Na ₃ PS ₄ (cubic)	2 × 10 ⁻⁴	Glass–ceramic	Hayashi et al., (2012b)
60Na ₂ S·40GeS ₂	7.3 × 10 ⁻⁶	Glass	Souquet et al. (1981)

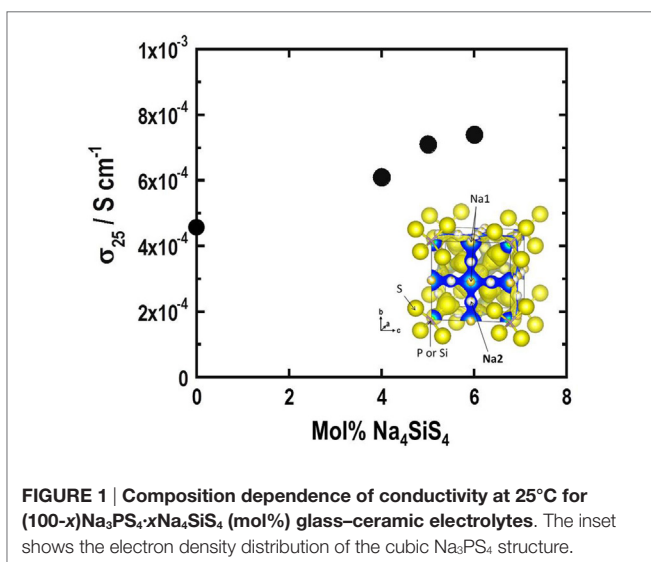


FIGURE 1 | Composition dependence of conductivity at 25°C for (100-x)Na₃PS₄·xNa₄SiS₄ (mol%) glass–ceramic electrolytes. The inset shows the electron density distribution of the cubic Na₃PS₄ structure.

Na⁺ ion conduction paths along Na1 and Na2 sites. Increased Na⁺ ion concentration is presumed as the reason for the enhancement of conductivity. Very recently, high conductivity of more than 10⁻³ S cm⁻¹ has been reported in crystalline Na₃PSe₄ (Zhang et al.,

2015). However, studies of new sulfide Na⁺ ion conductors are few. A first-principles calculation indicates that Sn-doped cubic Na₃PS₄ is predicted to have a higher Na⁺ ion conductivity of 10⁻² S cm⁻¹ (Zhu et al., 2015). Synthesis of SEs with a favorable structure for Na⁺ ion conduction based on calculation results is important for finding new Na⁺ ion conducting SEs.

Chemical Stability

A shortcoming of sulfide electrolytes is their lower chemical stability in air atmosphere. Sulfides tend to be decomposed by hydrolysis, generating harmful H₂S. Suppression of hydrolysis of sulfides is an important task for developing sulfide electrolytes. Based on our early experiments, the selection of compositions in sulfide electrolytes gives moderate stability in air to sulfide electrolytes (Muramatsu et al., 2011). The chemical stability of sulfide glass electrolytes in the binary system Li₂S–P₂S₅ was examined by exposing them to air atmosphere. Amounts of generated H₂S from the sulfides depend on the composition of the glasses; H₂S generation is minimized at the composition 75Li₂S·25P₂S₅ (mol%). The glass comprises Li⁺ and PS₄³⁻ ions. An isolated anion PS₄³⁻ without bridging sulfurs is useful for high tolerance for hydrolysis. Li₃PS₄-based SEs with both good chemical stability and high conductivity have been prepared by the combination of oxides (Li₂O or P₂O₅) and iodides (LiI) (Ohtomo et al., 2013a,b). The addition of metal oxides, such as ZnO, which act as an absorbent for H₂S, is also effective for decreasing H₂S (Hayashi et al., 2013). It is noteworthy that the use of a favorable M_xO_y (M_xO_y: Fe₂O₃, ZnO, and Bi₂O₃) with a larger negative Gibbs energy change (ΔG) for the reaction with H₂S is effective for improving the chemical stability of sulfide electrolytes. Another approach is the use of sulfide compositions based on the hard and soft acids and bases theory (HSAB; Sahu et al., 2014). Lithium tin thiophosphate, Li₄SnS₄, has better air stability than that of Li₃PS₄. Actually, as-substituted Li₄SnS₄ has good features of both high conductivity of 10⁻³ S cm⁻¹ and high air stability.

The chemical stability of SEs tends to affect battery performance. The electrochemical performance of all-solid-state C/LiCoO₂ cells using Li₃PS₄ glass or Li₇P₃S₁₁ glass–ceramic as a SE is compared. The cell with Li₃PS₄ glass electrolytes exhibits better cycle performance, although Li₃PS₄ glass has lower conductivity than Li₇P₃S₁₁ electrolyte (Ohtomo et al., 2013c). High performance of the battery would be based on the higher chemical stability of Li₃PS₄ electrolytes. Chemical stability as well as conductivity is an important factor of SEs for developing superior solid-state batteries.

Mechanical Property

Adhesion of the solid–solid interface is a key to the utilization of electrode active materials in all-solid-state batteries. Formability or processability of SEs is examined by the molding pressure dependence of the relative density of compressed powder pellets.

Figure 2A shows the dependence of the relative density of 75Li₂S·25P₂S₅ and 75Na₂S·25P₂S₅ (mol%) glass electrolytes on molding pressure. The relative densities increase gradually with an increase in molding pressure in both glasses at the same alkali compositions of 75 mol% M₂S (M = Li or Na), whereas the relative density for the Na₂S system is higher than that for the Li₂S

system (Sakuda et al., 2013a,b; Nose et al., 2015). Cross-sectional SEM images of the 75 mol% M_2S pellets pressed at 360 MPa are shown in the inset. Grain boundaries and voids in the pellets are more decreased in the 75Na₂S·25P₂S₅ glass compared with the 75Li₂S·25P₂S₅ glass. Sulfide glasses are densified by cold pressing without heat treatment, and this densification phenomenon is called “room-temperature pressure sintering” (Sakuda et al., 2013a,b). It is noteworthy that the 75Na₂S·25P₂S₅ glass has better formability than the 75Li₂S·25P₂S₅ glass. Both the glasses comprise Li⁺ or Na⁺ ion and PS₄³⁻ ion, which are thought to diffuse at the particle boundaries on pressing at room temperature. Na⁺ ion with a larger ionic radius than Li⁺ ion has a weaker interaction with PS₄³⁻ ion. Therefore, both Na⁺ and PS₄³⁻ ions would diffuse readily by cold press, leading to better densification.

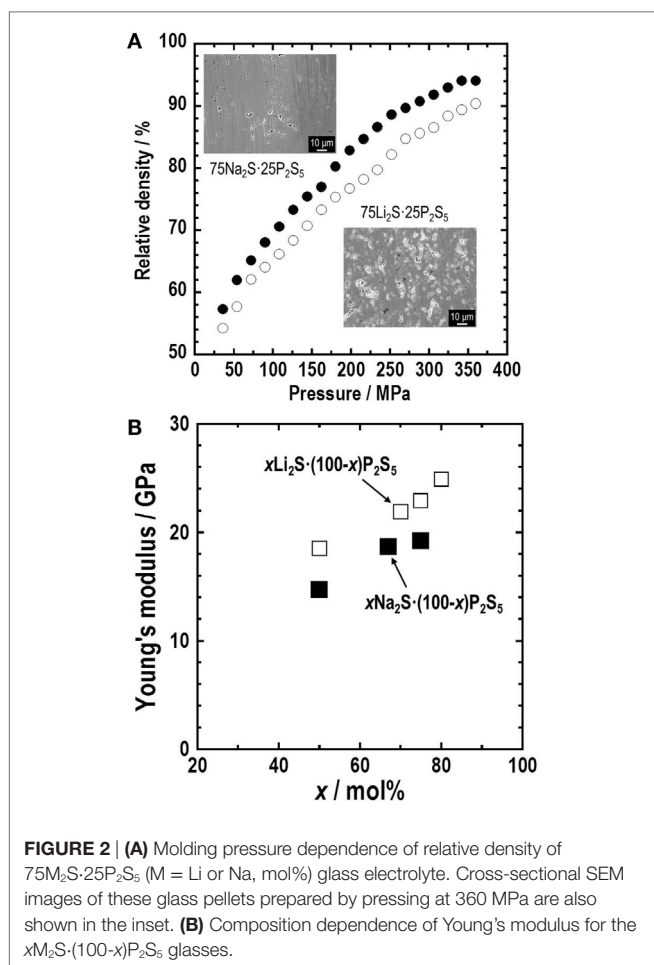
Retaining solid–solid contacts between active materials and SEs during charge–discharge processes brings about long cycle lives of all-solid-state batteries. Young’s moduli of SEs are important for keeping favorable contacts even at volume changes of active materials. Those for densified sulfide electrolytes prepared by hot-pressing are determined by an ultrasonic pulse-echo technique and the uniaxial compression tests (Sakuda et al., 2013a,b; Nose et al., 2015). Young’s moduli of the sulfide glasses in the systems Li₂S–P₂S₅ and Na₂S–P₂S₅ are presented in **Figure 2B**. They are increased gradually with the increase in the alkali content in

both systems. The Na₂S–P₂S₅ glasses have smaller Young’s moduli of 15–19 GPa than the Li₂S–P₂S₅ glasses (18–25 GPa). The difference on Young’s modulus is understood based on the Coulomb force and the mean atomic volume of the glasses. These sulfide glasses have an intermediate Young’s modulus between oxide glasses and organic polymers. Sulfide electrolytes deforming elastically are expected to act as a buffer in response to volume changes of active materials during charge–discharge processes. In fact, most all-solid-state batteries that use sulfide SEs exhibit good cycle performance.

Preparation Process

Sulfide SEs were prepared *via* various techniques. Crystalline electrolytes are prepared *via* solid-phase reaction, whereas glass electrolytes are obtained using the melt-quenching method. In general, sulfide starting materials are sealed in a carbon-coated quartz tube under vacuum and then heat-treated because of high vapor pressure of sulfides at high temperatures. Heating temperatures and cooling rates at preparation process affect precipitated crystals. A phase diagram in ternary system Li₂S–GeS₂–P₂S₅ is complicated (Hori et al., 2015), and crystalline Li₁₀GeP₂S₁₂ with a conductivity of 10^{−2} S cm^{−1} is prepared by selecting experimental conditions. Another preparation technique of sulfide electrolytes is mechanical milling using a high-energy planetary ball mill apparatus. This technique is fundamentally a room-temperature process. Therefore, sulfides are reacted at ordinary temperature and pressure. Electrolyte particles are obtained directly by milling. They are applicable to all-solid-state batteries without additional pulverization of electrolytes. Crystallization of glass electrolyte tends to precipitate a metastable phase, such as high-temperature phase, which generally has high ionic conductivity (Tatsumisago et al., 1991; Hayashi et al., 2003). Crystalline Li₇P₃S₁₁ (a high-temperature phase at the composition) is precipitated as a primary phase by heat treatment of a corresponding mother glass, and the obtained glass–ceramic electrolytes show conductivities of 10^{−3}–10^{−2} S cm^{−1}, which depend on the degree of crystallinity and the grain boundary of Li₇P₃S₁₁ (Mizuno et al., 2005, 2006; Seino et al., 2014). Cubic Na₃PS₄ is crystallized from the Na₃PS₄ glass prepared by mechanical milling. The prepared glass–ceramic electrolytes with Na₃PS₄ show Na⁺ ion conductivity of 10^{−4} S cm^{−1} at 25°C (Hayashi et al., 2012b).

Electrolyte preparation *via* liquid phase is a suitable process for cost-effective quantity synthesis without using a special reaction apparatus. In general, this process has benefits of lowering the reaction temperature, shortening the reaction time, and controlling the particle morphology and size. Prepared electrolyte solutions are also useful for the coating of active material particles. Very recently, liquid-phase synthesis of sulfide SEs has been reported. The reaction processes for sulfides are divided into two categories: one uses suspension and the other uses a homogeneous solution. For the former synthesis, β-Li₃PS₄ synthesized in tetrahydrofuran (Liu et al., 2013) or dimethyl carbonate (Phuc et al., 2016) as reaction medium and Li₇P₃S₁₁ synthesized in 1,2-dimethoxyethane (Ito et al., 2014) are reported. In these reactions, precursors with precipitates are obtained. Compressed pellets of the heat-treated sulfide electrolytes show conductivity of greater than 10^{−4} S cm^{−1} at 25°C. As the latter one *via*



homogeneous liquid, Li_3PS_4 is synthesized from a mixture of Li_2S and P_2S_5 with *N*-methylformamide (NMF) (Teragawa et al., 2014a). The Li_3PS_4 SEs can also be prepared using a dissolution–reprecipitation process in NMF from 80 Li_2S –20 P_2S_5 (mol%) glass prepared in advance using mechanical milling (Teragawa et al., 2014b). The prepared Li_3PS_4 electrolyte shows low conductivity of 10^{-6} S cm^{-1} at the present stage, but conductivity can be enhanced by selecting electrolyte compositions. Argyrodite-type $\text{Li}_6\text{PS}_5\text{Cl}$ is dissolved into ethanol. Then, the argyrodite phase is reprecipitated by removing ethanol at 80°C under vacuum for 3 h (Yubuchi et al., 2015a,b). A pellet of the product shows conductivity of 10^{-5} S cm^{-1} at 25°C, which is somewhat lower than that of the original $\text{Li}_6\text{PS}_5\text{Cl}$. Grain boundary resistance, which is affected by surface structure and morphology, might be greater in the prepared $\text{Li}_6\text{PS}_5\text{Cl}$. Optimization of posttreatments for the prepared powders will enhance the $\text{Li}_6\text{PS}_5\text{Cl}$ conductivity. Furthermore, the combination of sulfide SEs and ionic liquids produces pseudo-SEs (Minami et al., 2010; Oh et al., 2015). The prepared electrolytes give a new category of electrolytes having both high conductivity and good formability.

Sodium-ion conducting sulfide electrolytes with cubic Na_3PS_4 are also synthesized *via* a liquid-phase process from the mixture of Na_2S and P_2S_5 in NMF solvent (Yubuchi et al., 2015a). The room-temperature conductivity of the obtained electrolyte is 10^{-6} S cm^{-1} , which is lower than the conductivity of the electrolyte prepared by mechanical milling. Studies investigating sulfide SEs with Na^+ ion conductivity are extremely few at present. New electrolytes produced *via* a simple liquid-phase process will be researched widely.

PREPARATION OF SOLID–SOLID INTERFACE IN ALL-SOLID-STATE BATTERIES

Sulfide glasses are well-balanced SEs with high conductivity, good formability, appropriate Young's modulus, and moderate chemical stability. They are therefore highly promising SEs for use in all-solid-state batteries. A schematic diagram of bulk-type all-solid-state batteries is depicted in **Figure 3**. A positive electrode layer is composed not only of active material particles but also of SE ones. The Li^+ ion is supplied from SEs attached to active materials. Electrons are mobile through active materials. To enhance the rate of performance of the batteries, conductive additives of nanocarbons are added to the electrode layer. A lithium alloy or lithium metal is used as the negative electrode. A SE layer as a separator is sandwiched with the positive and negative electrode layers. Then, because of good formability of sulfide SEs, it can be pressed uniaxially at room temperature to fabricate bulk-type all-solid-state batteries.

An all-solid-state In/ LiCoO_2 or Li-In/ $\text{Li}_4\text{Ti}_5\text{O}_{12}$ cell with Li_2S – P_2S_5 glass–ceramic electrolytes exhibits good cycle performance for hundreds of times at 25°C (Tatsumisago and Hayashi, 2008; Tatsumisago et al., 2013). These cells operate at a high temperature of 100°C, where it is difficult for a liquid electrolyte cell to be used. The all-solid-state cell with $\text{Li}_4\text{Ti}_5\text{O}_{12}$ shows a discharge–charge capacity of about 140 mAh g^{-1} . It retains the capacity for 700

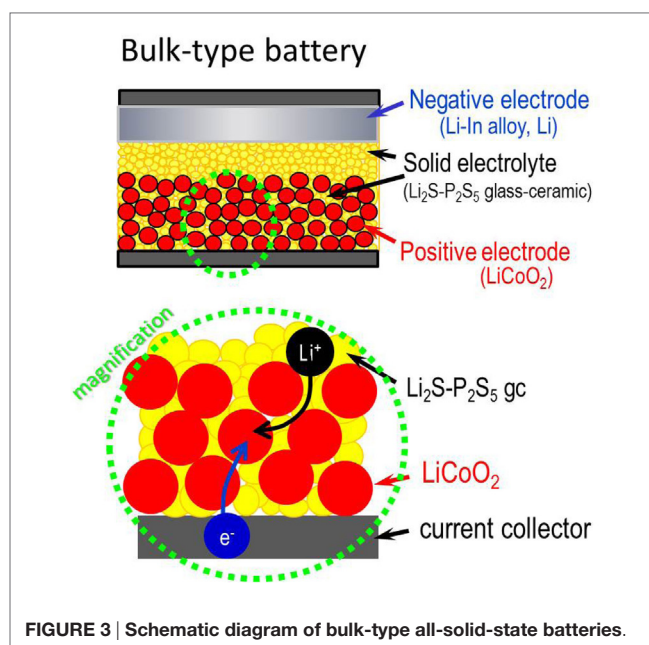


FIGURE 3 | Schematic diagram of bulk-type all-solid-state batteries.

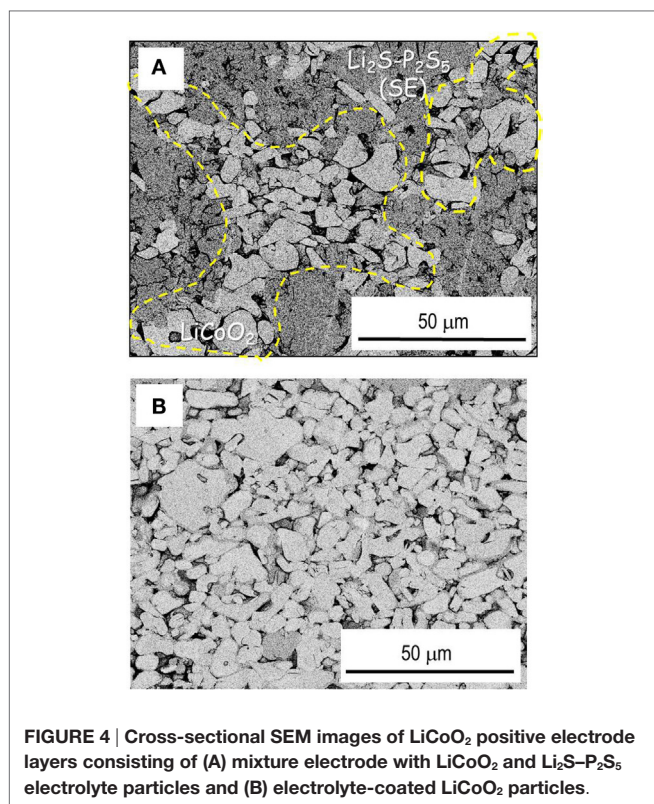
cycles with no degradation under a high current density of more than 10 mA cm^{-2} (Minami et al., 2011).

Coating of Sulfide Electrolytes on LiCoO_2 and Graphite Particles

Direct coating of sulfide SEs on LiCoO_2 particles, instead of mixing electrolyte particles, is effective for forming good electrolyte– LiCoO_2 interfaces with a wide contact area. Pulsed laser deposition (PLD) was first used as a coating technique (Sakuda et al., 2010, 2011). In this study, LiNbO_3 -coated LiCoO_2 particles were fluidized with a vibrator to ensure uniform coating of sulfide electrolytes on the particles.

Figure 4 presents cross-sectional SEM images of positive electrodes with (a) a conventional mixture of LiCoO_2 and Li_2S – P_2S_5 SE particles with the weight ratio of 70/30 and (b) SE-coated LiCoO_2 particles, where the weight ratio of LiCoO_2 and SE coatings was 90/10. **Figure 2A** shows that solid–solid contacts between LiCoO_2 and SE are formed by cold pressing of the mixture electrode because SE particles are deformed easily by pressing. **Figure 4A** shows that the aggregation of LiCoO_2 particles engenders less utilization of LiCoO_2 because many voids and less contact with SE are observed among LiCoO_2 particles. A close-packed electrode layer is formed using only SE-coated LiCoO_2 (**Figure 4B**). Its enlarged figure, which will be displayed in **Figure 7D** later, shows that a close solid–solid interface with fewer voids appears, and Li^+ ion conduction paths are therefore formed among LiCoO_2 particles. It is noteworthy that SE amounts in the electrode are decreased considerably by SE coating on LiCoO_2 particles. The use of minimum amounts of SE in an electrode layer contributes to enhanced energy density of all-solid-state batteries.

A cross-sectional high-angle annular dark field (HAADF)-STEM image and EDX mappings of O, P, S, Co, and Nb elements for the SE-coated LiCoO_2 electrodes are presented in **Figure 5**. A SE coating layer is observed between two LiCoO_2 particles,



where one particle has several cracks. The EDX mapping of Nb element reveals that a LiNbO₃ coating layer exists on the surface of LiCoO₂, but the layer is missing at the cracks. The EDX mappings of P and S elements indicate that SE penetrates into the cracks as a liquid electrolyte does. Favorable formability of sulfide SE is effective for forming good contacts with the surface of active materials and using active materials even at newly formed crystal faces with cracks.

Solid electrolyte coatings were also done for graphite particles using PLD. The mixture of SE-coated graphite and SE particles was used as a negative electrode. The weight ratio of graphite and SE was 90/10. All-solid-state cells with Li₂S–P₂S₅ SE as a separator layer were charged and discharged at a constant current density of 0.064 mA cm⁻² (ca. 0.05 C) for voltages of 2.8–4.3 or 4.6 V at room temperature (Sakuda et al., 2013b). **Figure 6** shows charge–discharge curves for all-solid-state SE-coated graphite/SE-coated LiCoO₂ batteries. The battery with a cutoff voltage of 4.6 V at the charge process shows a higher discharge capacity than that of 4.3 V. Battery has a discharge capacity of 133 mAh g⁻¹, as calculated from the total mass of the composite positive electrode.

Figure 7 shows cross-sectional SEM images of SE-coated LiCoO₂ positive electrodes; **Figure 7A** as-prepared, **Figure 7B** after the initial charge–discharge (cutoff voltage: 4.3 V), and **Figure 7C** after the initial charge–discharge (cutoff voltage: 4.6 V). **Figures 7D–F**, respectively, portray enlarged images of **Figures 7A–C**. Closely attached SE–LiCoO₂ interfaces with large contact area are achieved by PLD coating, as shown in **Figures 7A,D**. The electrode morphology (**Figure 7B**) does not change greatly after the initial charge–discharge process at the

cutoff of 4.3 V. SE coatings still attach on the LiCoO₂ particles (**Figure 7E**), and empty spaces among particles observed in panel (**Figure 7B**) are similar to those observed in the as-prepared electrode (**Figure 7A**). **Figure 7C** shows that voids among LiCoO₂ particles increase after the charge–discharge process at a higher cutoff voltage of 4.6 V. A LiCoO₂ particle charged to 4.6 V suffers from deterioration. Many cracks are formed in the particle, as shown in the magnified image of panel (**Figure 7F**). This morphological change is attributable to (1) reduction of mechanical strength and (2) excess strain at the solid–solid interfaces among LiCoO₂ particles during their large volume expansion and/or phase transition.

Figure 8 shows cross-sectional SEM images of SE-coated graphite negative electrodes; **Figure 8A** as-prepared and **Figure 8B** after the initial charge–discharge (cutoff voltage: 4.3 V). Graphite particles are close-packed in a negative electrode layer. SE coatings are observed around graphite particles. They form Li⁺ ion conduction paths through the electrode layer. After the initial charge–discharge, no obvious void is observed in the negative electrode. The close-packed electrode is present. Good solid–solid interfaces are also retained between the graphite layer and an electrolyte separator layer.

As described in Section “Preparation Process,” liquid-phase synthesis of sulfide electrolytes is also useful for forming favorable electrode–electrolyte solid–solid interfaces, which can be achieved by removing solvents from electrolyte solutions. An all-solid-state cell using LiCoO₂ coated with Li₃PS₄ electrolyte *via* an NMF solution operates as rechargeable batteries without the addition of SE and carbon-conductive additive particles to the positive electrodes (Teragawa et al., 2014a,b). However, the cell capacities are lower than those of the cells using LiCoO₂ coated with Li₃PS₄ electrolytes by PLD, because the electrolytes synthesized *via* the liquid-phase has lower ionic conductivities than those prepared by PLD. The LiCoO₂ particles coated with Li₆PS₅Cl electrolytes *via* ethanol solution with a higher conductivity than Li₃PS₄ were therefore applied to all-solid-state cells. The weight ratio of LiCoO₂/SE layer was 92.5/7.5 in SE-coated LiCoO₂ particles. An all-solid-state cell using the electrolyte-coated LiCoO₂ shows an initial discharge capacity of 45 mAh g⁻¹, which is greater than that of cells using Li₃PS₄-coated LiCoO₂ (Yubuchi et al., 2015b). SE coating *via* electrolyte liquids is a simple and cost-effective process. Increasing conductivity of SE at lower temperatures is necessary to improve battery performance.

Sulfur-Based Nanocomposite Positive Electrodes

Sulfur is a fascinating positive electrode with high energy density because it is an abundant resource with high theoretical capacity of 1672 mAh g⁻¹ and environmental friendliness. Lithium polysulfides (Li₂S_x), which are formed during discharge (lithiation process), are readily dissolved in organic liquid electrolytes, leading to lack of a sulfur positive electrode. Dissolution of lithium polysulfides is suppressed by absorbing sulfurs in nano-carbon pores. This approach has been studied extensively (Ji and Nazar, 2010). The use of inorganic SEs fundamentally resolves the problem.

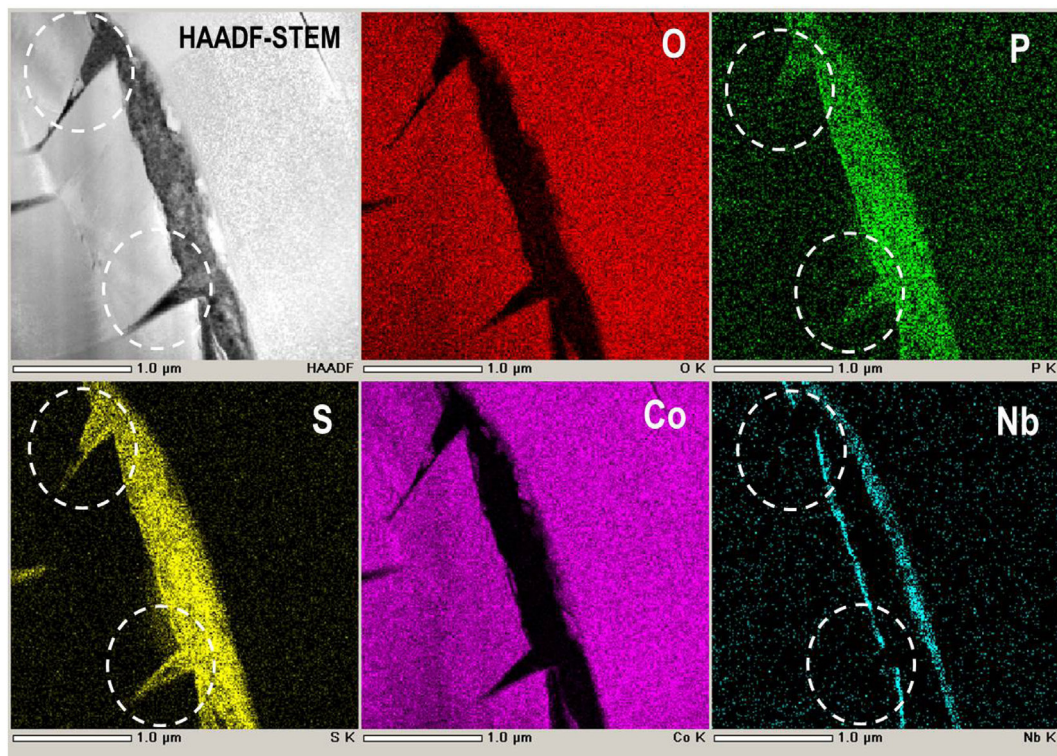


FIGURE 5 | Cross-sectional high-angle annular dark field (HAADF)-TEM image and EDX mappings of O, P, S, Co, and Nb elements for the SE-coated LiCoO_2 electrodes.

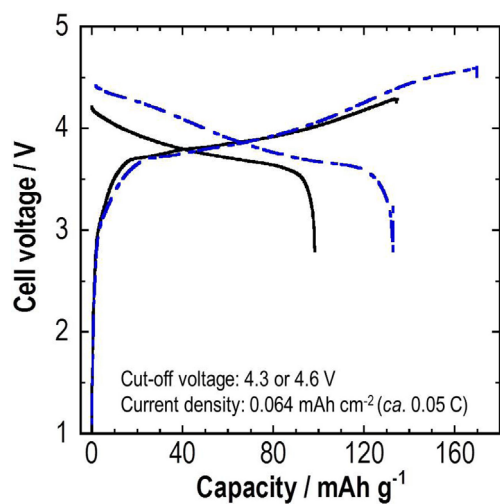


FIGURE 6 | Initial charge-discharge curves for an all-solid-state SE-coated graphite/SE-coated LiCoO_2 battery.

Composite sulfur electrodes consisting of S, acetylene black (AB), and $\text{Li}_2\text{S-P}_2\text{S}_5$ SE powders with a weight ratio of 25/25/50 were prepared using high-energy planetary ball milling to produce favorable contacts among the three components (Nagao et al., 2011). The Li-In/S cell exhibits a large reversible capacity of

greater than 1500 mAh g^{-1} of sulfur with average potential of ca. 2.1 V (vs. Li^+/Li). The cell with sulfur electrode shows 15 times higher capacity than the cell with LiCoO_2 , although the operating potential of the former cell is almost half that of the latter cell.

Application of Li_2S as a discharge product of sulfur active material offers the important benefits of high theoretical capacity of 1167 mAh g^{-1} and versatility of negative electrode materials without lithium sources. Because of the insulative nature of Li_2S , composite electrodes, Li_2S mixed with conductive additives, such as nanocarbons and SEs, should be prepared for the use of Li_2S as an active material. Composite Li_2S electrodes were prepared by mechanical milling. A typical weight ratio of $\text{Li}_2\text{S}/\text{AB}/\text{Li}_2\text{S-P}_2\text{S}_5$ SE is 25/25/50. The prepared composite gives broad peaks attributable to Li_2S in X-ray diffraction patterns. An all-solid-state cell of In/ Li_2S composites is charged and then discharged at 25°C . The initial reversible capacity is 800 mAh g^{-1} at the current density of 0.064 mA cm^{-2} (Nagao et al., 2012b). The cell retained 750 mAh g^{-1} for 10 cycles. Charge-discharge reaction mechanisms were examined using high-resolution TEM observation (Nagao et al., 2015). **Figure 9** shows TEM images for the Li_2S electrodes; **Figure 9A** before charge-discharge test, **Figure 9B** after the initial charge, and **Figure 9C** after the initial discharge. **Figure 9A** shows that nanoparticles of ca. 5 nm in size with different crystal orientations are distributed randomly in the matrix consisting of amorphous SE and AB. Those nanoparticles are attributable to crystalline Li_2S . **Figure 9B** shows that no lattice fringes because of the crystalline Li_2S are apparent, and

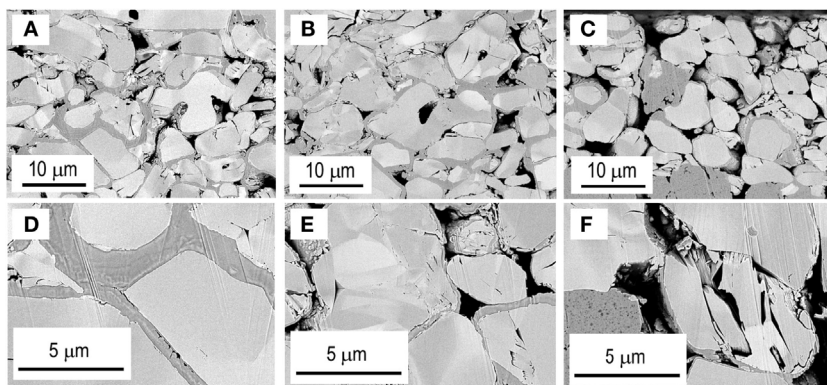


FIGURE 7 | Cross-sectional SEM images of SE-coated LiCoO_2 positive electrodes (A) as-prepared, (B) after the initial charge–discharge (cutoff voltage: 4.3 V), and (C) after the initial charge–discharge (cutoff voltage: 4.6 V). Images of (D–F), respectively, depict enlarged images of (A–C).

there exists the characteristic contrast attributable to amorphous structure in the whole region after the initial charge process. As shown in **Figure 9C**, lattice fringes with spacing of about 3.9 \AA are clearly apparent after the initial discharge, suggesting that amorphous sulfur is converted into crystalline nanoparticles during discharge reaction. Reversible transformation between crystallization and amorphization of sulfur-based active nanoparticles is responsible for the high capacity and its retention.

The utilization of Li_2S is ca. 50% in the composite electrode. To increase the utilization of Li_2S , one strategy is the fundamental enhancement of ionic conductivity in Li_2S . A partial substitution of more polarizable iodide anion with larger ionic radii for sulfide anion in Li_2S is expected to increase conductivity by introducing lithium vacancies and by increasing the lattice constant. Solid solutions in the system Li_2S -LiI are therefore prepared using mechanical milling (Hakari et al., 2015a). Only the XRD peaks attributable to Li_2S are observed; LiI peaks disappear completely in the composition range of $0 < \text{LiI (mol\%)} < 20$. **Figure 10A** presents the composition dependence of lattice constant and conductivity at 25°C for the prepared Li_2S -LiI materials. The lattice constant increases monotonically with increased LiI content, suggesting that Li_2S -based solid solutions are prepared using a mechanical milling process. Conductivity is also enhanced by increasing the LiI content. The solid solution with 20 mol% LiI has conductivity of $2.2 \times 10^{-6} \text{ S cm}^{-1}$, which is two orders of magnitude higher than that for Li_2S itself without the addition of LiI. A composite positive electrode with the $80\text{Li}_2\text{S}\cdot 20\text{LiI}$ (mol%) solid solution, vapor-grown carbon fiber (VGCF), and Li_3PS_4 glass electrolyte with a weight ratio of 50/10/40 is applied to all-solid-state cells. **Figure 10B** shows that an all-solid-state cell (Li-In/ $\text{Li}_3\text{PS}_4/80\text{Li}_2\text{S}\cdot 20\text{LiI}$) is charged and discharged at a current density of 0.13 mA cm^{-2} (0.07 C) at 25°C . The cell shows a reversible capacity of 930 mAh g^{-1} for 50 cycles. The capacity corresponds to 80% utilization of Li_2S . It is noteworthy that the enhancement of conductivity of Li_2S is effective for increasing the utilization of the active material. This strategy is beneficial for the development of all-solid-state cells with a higher energy density.

A SE Li_3PS_4 is ball-milled with nanocarbon, such as AB. The prepared Li_3PS_4 -AB materials as a mixed conductor are useful

as positive electrode acting not only as a SE but also as an active material. An all-solid-state cell with the Li_3PS_4 -AB composite positive electrode is charged and discharged. Its operation voltage of ca. 2.6 V vs. Li^+/Li is somewhat higher than that of Li_2S (Hakari et al., 2015b). Redox-active electrolytes, such as CuCl_2 -dissolved solution in porous carbons, are also reported to apply to supercapacitors (Mai et al., 2013). The use of the SEs as an active material in electrode layers is effective at increasing the reversible capacity per gram of the total mass of positive electrodes.

Transition Metal Sulfide Positive Electrodes

Typical MS_x , such as TiS_2 , are used as active materials in all-solid-state Li and Na batteries with sulfide SEs. Decreasing the particle size of MS_x and forming a wide contact area with both SEs and conductive additives are important for increasing the MS_x utilization.

Monodispersed MS_x nanoparticles are prepared using a so-called “hot-soap” technique using high-boiling point solvents as a reaction medium. Particle morphology and size can be controlled by choosing the reaction conditions and combinations of coordinating or non-coordinating solvents. NiS particles of 50 nm size were prepared using thermal decomposition of nickel acetylacetonate in a mixed solution of 1-dodecanethiol as a sulfur source and 1-octadecene as a non-coordinating solvent at 280°C for 5 h (Aso et al., 2011). The NiS nanoparticles are crystallized directly on a carbon fiber (VGCF) by adding VGCF to a liquid medium. Good adhesion between NiS and carbon is achieved (Aso et al., 2012). Sulfide electrolyte coating on NiS-VGCF was produced using the PLD method. All-solid-state cells with the prepared NiS composite electrode operate as a secondary battery at 25°C , suggesting that electron and Li^+ ion conduction paths are formed in the composite electrodes (Aso et al., 2013).

To increase the positive electrode capacity, sulfur-rich MS_x are desired. For example, titanium trisulfide TiS_3 shows a higher capacity than that of TiS_2 , because additional sulfurs in TiS_3 contribute to the redox reaction that occurs during charge–discharge processes (Hayashi et al., 2012a). Amorphous NbS_x ($x = 3, 4, 5$)

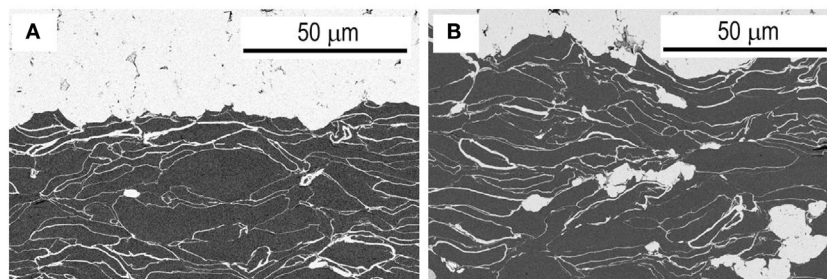


FIGURE 8 | Cross-sectional SEM images of SE-coated graphite negative electrodes (A) as-prepared and (B) after the initial charge–discharge (cutoff voltage: 4.3 V).

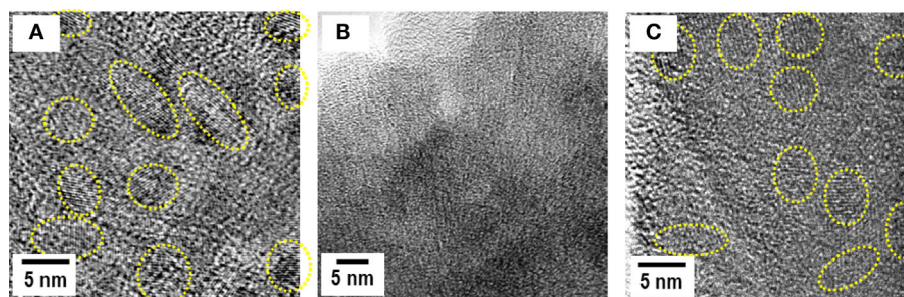


FIGURE 9 | TEM images for the Li_2S electrodes (A) before charge–discharge test, (B) after the initial charge, and (C) after the initial discharge.

are prepared mechanochemically. Electrochemical cells with an organic liquid electrolyte using the amorphous NbS_x ($x = 3, 4, 5$) show higher discharge capacities with an increase in the sulfur content of NbS_x (Sakuda et al., 2014). Amorphous TiS_3 ($a\text{-TiS}_3$) retains a higher capacity than crystalline TiS_3 in all-solid-state lithium cells. The crystal structure of TiS_3 is partially deteriorated at the initial cycle, leading to an irreversible capacity in the cell with crystalline TiS_3 (Matsuyama et al., 2016a,b). It is noteworthy that sulfur-rich amorphous MS_x with electrical conductivity are promising for use as positive electrodes instead of sulfur active materials.

Figure 11A shows the first and tenth charge–discharge curves of all-solid-state lithium cell $\text{Li-In}/a\text{-TiS}_3$ at 0.013 mA cm^{-2} at 25°C . The right side ordinate axis represents the electrode potential vs. Li^+/Li , as calculated based on the potential difference between the Li-In and Li electrode (0.62 V). The cell with $a\text{-TiS}_3$ positive electrode including no carbon-conductive additives and SEs shows a reversible capacity for 10 cycles of about 510 mAh g^{-1} of $a\text{-TiS}_3$, which equals the weight of the total positive electrode. The capacity corresponds to storage of about 3M Li to $a\text{-TiS}_3$. Electronic structural analyses using S2p XPS and S K -edge XANES reveal that a reversible sulfur redox in $a\text{-TiS}_3$ appears mainly during charge–discharge processes and contributes to its good capacity retention (Matsuyama et al., 2016a,b).

Amorphous TiS_3 is also applicable to all-solid-state sodium batteries. An all-solid-state sodium cell using $a\text{-TiS}_3$ shows capacity higher than 300 mAh g^{-1} at the first discharge process,

as presented in **Figure 11B** (Tanibata et al., 2015a). The composite positive electrode consisting of $a\text{-TiS}_3$ and the cubic Na_3PS_4 electrolyte with a weight ratio of 40/60 is used. $\text{Na}_{15}\text{Sn}_4$ alloy and the cubic Na_3PS_4 electrolyte are used, respectively, as a negative electrode and a separator layer. The cell capacity decreases gradually during discharge–charge cycles. SEM–EDX analysis reveals that the $a\text{-TiS}_3$ particles aggregate after the cycles, and that resistance in the $a\text{-TiS}_3$ composite electrode increases during cycles. To secure electron conduction paths to $a\text{-TiS}_3$, 6 wt% AB is added to the positive electrode. Good capacity retention is achieved in the cell using $a\text{-TiS}_3$ electrode with AB. The added AB particles might prevent the shutoff of electron conduction paths in the composite electrode and give a buffer space for the volume change of $a\text{-TiS}_3$ particles for preserving adhesion among the particles. The addition of AB to the $\text{Na}_{15}\text{Sn}_4$ electrode also suppresses cell resistance after charge–discharge. In addition, the replacement of Na_3PS_4 glass–ceramic by $94\text{Na}_3\text{PS}_4\cdot 6\text{Na}_4\text{Si}_4$ (mol%) glass–ceramic with higher conductivity decreases cell resistance and increases the rate performance of all-solid-state cells (Tanibata et al., 2015b). Reversible capacity in all-solid-state Na cells is less than that in all-solid-state Li cells, as shown in **Figures 11A,B**. The lower conductivity of SEs and loss of particle contacts because of the larger volume change are responsible for a smaller capacity for the Na cells. Approaches that are used to prepare composite positive electrodes suitable for insertion/de-insertion of Na^+ ion with larger ionic radius must be developed to improve battery performance in all-solid-state Na batteries.

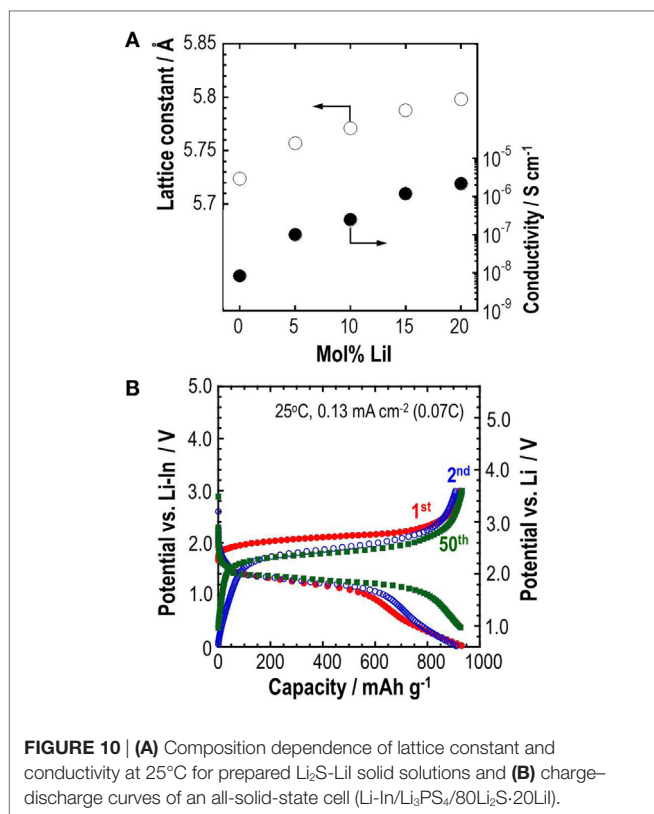


FIGURE 10 | (A) Composition dependence of lattice constant and conductivity at 25°C for prepared Li_2S -LiI solid solutions and **(B)** charge-discharge curves of an all-solid-state cell (Li-In/ Li_3PS_4 /80 Li_2S -20LiI).

Interface Modification for Li Metal Negative Electrode

To achieve high energy density of all-solid-state Li batteries, the final goal is the use of lithium metal as a negative electrode. Lithium metal is an ultimate negative electrode because of a large theoretical capacity of 3861 mAh g^{-1} and the lowest electrochemical potential of -3.04 V vs. SHE. However, a possibility of fatal problems emerged by short-circuit with dendrite formation prevent the practical use of Li metal negative electrode in lithium cells with conventional liquid and polymer electrolytes. Combination with inorganic SEs is expected to resolve the problem. In fact, thin-film solid-state batteries with Li negative electrode have excellent cycle life without capacity fading (Bates et al., 1993). The rate of utilization of Li electrodes is not high in thin-film batteries because positive electrodes such as LiCoO_2 have lithium sources, which are mainly used for a charge-discharge process.

Compared with thin-film batteries fabricated by gas-phase deposition, insufficient Li-SE interfaces in bulk-type all-solid-state batteries prepared by cold pressing are important issues that must be resolved. It has been revealed by *in situ* SEM observation that lithium is deposited through grain boundaries and voids in the SE (Nagao et al., 2013). Insertion of a Li-alloy thin layer at the interface between the Li electrode and SE layers brought about stable Li dissolution and deposition in the all-solid-state Li metal cells (Hiratani et al., 1988; Okita et al., 2011; Nagao et al., 2012a). These interface modifications are effective at establishing homogeneous interfaces between the Li metal and SEs.

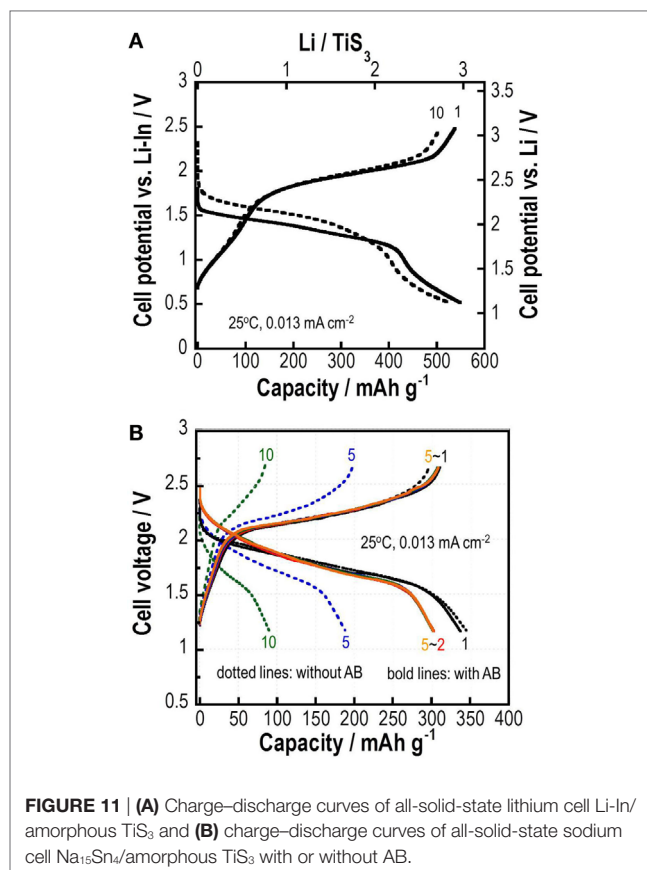


FIGURE 11 | (A) Charge-discharge curves of all-solid-state lithium cell Li-In/amorphous TiS_3 and **(B)** charge-discharge curves of all-solid-state sodium cell $\text{Na}_{15}\text{Sn}_4$ /amorphous TiS_3 with or without AB.

Intensive utilization of Li is important for achieving high energy density of all-solid-state lithium metal batteries. Insertion of a Au thin film at the Li-SE interface is effective for increasing Li utilization (Kato et al., 2016a). Li and Au thin films were formed on a pelletized Li_3PS_4 glass electrolyte by vacuum evaporation. Galvanostatic cycling tests for the Li/ Li_3PS_4 /Li cell are presented in **Figure 12A**. At the initial cycle, the utilization of Li metal is about 40%, which is a higher rate of utilization of Li metal for thin-film batteries (about 20%). However, utilization of Li metal for the cell decreases rapidly after five cycles. The Li thin-film morphology is rough after galvanostatic cycling tests, as shown in the SEM image (**Figure 12C**), indicating that inhomogeneous Li dissolution-deposition reactions occur. The cell Li/Au/ Li_3PS_4 /Au/Li has about 35% Li utilization at the initial cycle and retains about 25% after the fifth cycle, as presented in **Figure 12B**. The morphology of Li metal after Li dissolution-deposition reaction became more uniform, as shown in the SEM image of panel (**Figure 12D**), compared with the cell without Au thin films. The insertion of Au film to a Li-SE interface is a first step for improving the cyclability of Li deposition-dissolution reactions with high Li utilization in all-solid-state lithium metal batteries. Intensive studies are in progress.

CONCLUDING REMARKS

We have reviewed recent developments related to sulfide SEs and interface formation processes for all-solid-state rechargeable batteries. The conductivity of sulfide Li^+ ion conductors, such as

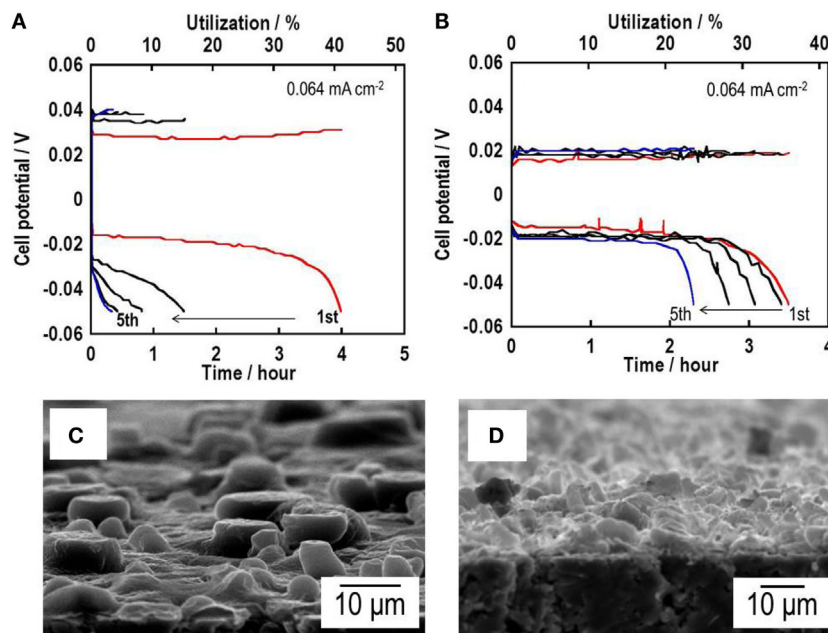


FIGURE 12 | Galvanostatic cycling tests for (A) a Li symmetric Li/Li₃PS₄/Li cell and (B) a Li/Au/Li₃PS₄/Au/Li cell. SEM images of the surface of (C) a Li/Li₃PS₄/Li cell and (D) a Li/Au/Li₃PS₄/Au/Li cell after galvanostatic cycling tests.

Li₁₀GeP₂S₁₂, Li₇P₃S₁₁, and Li_{9.54}Si_{1.74}P_{1.44}S_{11.7}Cl_{0.3}, has already reached 10⁻² S cm⁻¹ at room temperature. Conductivities of sulfide Na⁺ ion conductors are lower than those of Li⁺ ion conductors at the present stage. The highest conductivity of 10⁻³ S cm⁻¹ was obtained for Na₃PSe₄. Sulfide glass electrolytes with high alkali content were prepared by high-energy ball milling process. Metastable phases, such as Li₇P₃S₁₁ and cubic Na₃PS₄, with high conductivity were formed by careful crystallization of the prepared glasses. Sulfide electrolytes can be synthesized *via* liquid-phase processing, which is useful for coating application. Sulfide glass electrolytes have favorable formability, and Young's modulus for forming good electrode–electrolyte interfaces achieving rapid charge transfer in bulk-type all-solid-state batteries. Chemical stability in air is a great shortcoming of using a sulfide electrolyte. The composition of Li₃PS₄ has superior chemical stability in the Li₂S–P₂S₅ binary system. The higher chemical stability is achieved by partial substitution of oxygen for sulfur. Selecting composition and designing structure for sulfide electrolytes is expected to improve conductivity, mechanical properties, and chemical stability further. As Na⁺ ion conductors, higher conductivity of more than 10⁻² S cm⁻¹ is predicted for Sn-substituted cubic Na₃PS₄, but the conductivity has not been achieved experimentally. Further studies seeking new electrolytes and suitable preparation processes must be undertaken.

Coating of SE and preparation of nanocomposites are useful for forming favorable solid–solid interface in an electrode layer for bulk-type all-solid-state batteries. Coating of sulfide electrolytes on LiCoO₂ or graphite particles using gas-phase or liquid-phase techniques is effective for increasing solid–solid contact area using extremely small amounts of electrolytes. Preparation of nanocomposites using high-energy ball milling is useful for sulfur or Li₂S active materials with an insulative nature. Conductivity

enhancement of Li₂S by combination with LiI contributes to the improvement of Li₂S utilization. Amorphous MS_x, such as amorphous TiS₃, are attractive as mixed conductors with large capacity in all-solid-state batteries. Interface modification for Li metal negative electrode with Au thin film improves the cycle performance of Li dissolution–deposition while maintaining a high rate of utilization. For further improvement of electrochemical performance of the batteries, facile approaches achieving favorable electrode–electrolyte interfaces with large contact area will be developed. Controlling the size, morphology, and dispersibility of both electrolyte and electrode particles and selecting suitable electrolytes for maintaining close solid–solid contacts during charge–discharge processes will be assessed in future studies.

AUTHOR CONTRIBUTIONS

AH contributed to the preparation of the manuscript. AS and MT contributed to the discussions about research results.

ACKNOWLEDGMENTS

This research is supported by a Grant-in-Aid for Scientific Research from the Ministry of Education, Culture, Sports, Science and Technology (MEXT) of Japan. In particular, the research about all-solid-state Li batteries was financially supported by the Japan Science and Technology Agency (JST), Advanced Low Carbon Technology Research and Development Program (ALCA), Specially Promoted Research for Innovative Next Generation Batteries (SPRING) Project, while the research about all-solid-state Na batteries was supported by the MEXT program “Elements Strategy Initiative for Catalysts and Batteries (ESICB).”

REFERENCES

- Aotani, N., Iwamoto, K., Takada, K., and Kondo, S. (1994). Synthesis and electrochemical properties of lithium ion conductive glass, $\text{Li}_3\text{PO}_4\text{-Li}_2\text{S-SiS}_2$. *Solid State Ionics*. 68, 35–39. doi:10.1016/0167-2738(94)90232-1
- Aso, K., Hayashi, A., and Tatsumisago, M. (2012). Synthesis of NiS-carbon fiber composites in high-boiling solvent to improve electrochemical performance in all-solid-state lithium secondary batteries. *Electrochim. Acta* 83, 448–453. doi:10.1016/j.electacta.2012.07.088
- Aso, K., Kitaura, H., Hayashi, A., and Tatsumisago, M. (2011). Synthesis of nanosized nickel sulfide in high-boiling solvent for all-solid-state lithium secondary batteries. *J. Mater. Chem.* 21, 2987–2990. doi:10.1039/c0jm02639e
- Aso, K., Sakuda, A., Hayashi, A., and Tatsumisago, M. (2013). All-solid-state lithium secondary batteries using NiS-carbon fiber composite electrodes coated with $\text{Li}_2\text{S-P}_2\text{S}_5$ solid electrolytes by pulsed laser deposition. *ACS Appl. Mater. Interfaces* 5, 686–690. doi:10.1021/am302164e
- Bates, J., Dudney, N., Gruzalski, G., Zuhr, R., Choudhury, A., and Luck, C. (1993). Fabrication and characterization of amorphous lithium electrolyte thin films and rechargeable thin-film batteries. *J. Power Sources* 4, 103–110. doi:10.1016/0378-7753(93)80106-Y
- Boron, P., Johansson, S., Zick, K., Gunne, J., Dehnen, S., and Roling, B. (2013). $\text{Li}_{10}\text{SnP}_2\text{S}_{12}$: an affordable lithium superionic conductor. *J. Am. Chem. Soc.* 135, 15694–15697. doi:10.1021/ja407393y
- Boulineau, S., Courty, M., Tarascon, J. M., and Viallet, V. (2012). Mechanochemical synthesis of Li-argyrodite $\text{Li}_6\text{PS}_5\text{X}$ (X=Cl, Br, I) as sulfur-based solid electrolytes for all solid state batteries application. *Solid State Ionics*. 221, 1–5. doi:10.1016/j.ssi.2012.06.008
- Hakari, T., Hayashi, A., and Tatsumisago, M. (2015a). Highly utilized lithium sulfide active material by enhancing conductivity in all-solid-state batteries. *Chem. Lett.* 44, 1664–1666. doi:10.1246/cl.150758
- Hakari, T., Nagao, M., Hayashi, A., and Tatsumisago, M. (2015b). All-solid-state lithium batteries with Li_3PS_4 glass as active material. *J. Power Sources* 293, 721–725. doi:10.1016/j.jpowsour.2015.05.073
- Hayashi, A., Hama, S., Minami, T., and Tatsumisago, M. (2003). Formation of superionic crystals from mechanically milled $\text{Li}_2\text{S-P}_2\text{S}_5$ glasses. *Electrochem. Commun.* 5, 111–114. doi:10.1016/S1388-2481(02)00555-6
- Hayashi, A., Matsuyama, T., Sakuda, A., and Tatsumisago, M. (2012a). Amorphous titanium sulfide electrode for all-solid-state rechargeable lithium batteries with high capacity. *Chem. Lett.* 41, 886–888. doi:10.1246/cl.2012.886
- Hayashi, A., Noi, K., Sakuda, A., and Tatsumisago, M. (2012b). Superionic glass-ceramic electrolytes for room-temperature rechargeable sodium batteries. *Nat. Commun.* 3, 1–5. doi:10.1038/ncomms1843
- Hayashi, A., Muramatsu, H., Ohtomo, T., Hama, S., and Tatsumisago, M. (2013). Improvement of chemical stability of Li_3PS_4 glass electrolytes by adding M_2O_y (M=Fe, Zn, and Bi) nanoparticles. *J. Mater. Chem. A* 1, 6320–6326. doi:10.1039/c3ta10247e
- Hiratani, M., Miyachi, K., and Kudo, T. (1988). Effect of a lithium alloy layer inserted between a lithium anode and a solid electrolyte. *Solid State Ionics*. 2, 1406–1410. doi:10.1016/0167-2738(88)90394-3
- Hori, S., Kato, M., Suzuki, K., Hirayama, M., Kato, Y., and Kanno, R. (2015). Phase diagram of the $\text{Li}_4\text{GeS}_4\text{-Li}_3\text{PS}_4$ quasi-binary system containing the superionic conductor $\text{Li}_{10}\text{GeP}_2\text{S}_{12}$. *J. Am. Ceram. Soc.* 98, 3352–3360. doi:10.1111/jace.13694
- Ito, S., Nakakita, M., Aihara, Y., Uehara, T., and Machida, N. (2014). A synthesis of crystalline $\text{Li}_7\text{P}_3\text{S}_{11}$ solid electrolyte from 1, 2-dimethoxyethane solvent. *J. Power Sources* 271, 342–345. doi:10.1016/j.jpowsour.2014.08.024
- Jansen, M., and Henseler, U. (1992). Synthesis, structure determination, and ionic conductivity of sodium tetrathiosulfate. *J. Solid State Chem.* 99, 110–119. doi:10.1016/0022-4596(92)90295-7
- Ji, X., and Nazar, L. (2010). Advances in Li-S batteries. *J. Mater. Chem.* 20, 9821–9826. doi:10.1039/b925751a
- Kamaya, N., Homma, K., Yamakawa, Y., Hirayama, M., Kanno, R., Yonemura, M., et al. (2011). A lithium superionic conductor. *Nat. Mater.* 10, 682–686. doi:10.1038/nmat3066
- Kato, A., Hayashi, A., and Tatsumisago, M. (2016a). Enhancing utilization of lithium metal electrodes in all-solid-state batteries by interface modification with gold thin films. *J. Power Sources* 309, 27–32. doi:10.1016/j.jpowsour.2016.01.068
- Kato, Y., Hori, S., Saito, T., Suzuki, K., Hirayama, M., Mitsui, A., et al. (2016b). High-power all-solid-state batteries using sulfide superionic conductors. *Nat. Energy* 1, 16030. doi:10.1038/nenergy.2016.30
- Liu, Z., Fu, W., Payzant, E., Yu, X., Wu, Z., Dudney, N., et al. (2013). Anomalous high ionic conductivity of nanoporous $\beta\text{-Li}_3\text{PS}_4$. *J. Am. Chem. Soc.* 135, 975–978. doi:10.1021/ja3110895
- Mai, L. Q., Minhas-Khan, A., Tian, X., Hercule, K. M., Zhao, Y. L., Lin, X., et al. (2013). Synergistic interaction between redox-active electrolyte and binder-free functionalized carbon for ultrahigh supercapacitor performance. *Nat. Commun.* 4, 2923. doi:10.1038/ncomms3923
- Matsuyama, T., Deguchi, M., Mitsuhara, K., Ohta, T., Mori, T., Orikasa, Y., et al. (2016a). Structure analyses using X-ray photoelectron spectroscopy and X-ray absorption near edge structure for amorphous MS_3 (M: Ti, Mo) electrodes in all-solid-state lithium batteries. *J. Power Sources* 313, 104–111. doi:10.1016/j.jpowsour.2016.02.044
- Matsuyama, T., Hayashi, A., Ozaki, T., Mori, S., and Tatsumisago, M. (2016b). Improved electrochemical performance of amorphous TiS_3 electrodes compared to its crystal for all-solid-state rechargeable lithium batteries. *J. Ceram. Soc. Jpn.* 124, 242–246. doi:10.2109/jcersj2.15299
- Minami, K., Hayashi, A., and Tatsumisago, M. (2010). Characterization of solid electrolytes prepared from $\text{Li}_2\text{S-P}_2\text{S}_5$ glass and ionic liquids. *J. Electrochem. Soc.* 157, A1296–A1301. doi:10.1149/1.3489352
- Minami, K., Hayashi, A., Ujiie, S., and Tatsumisago, M. (2011). Electrical and electrochemical properties of glass-ceramic electrolytes in the systems $\text{Li}_2\text{S-P}_2\text{S}_5\text{-P}_2\text{S}_5$ and $\text{Li}_2\text{S-P}_2\text{S}_5\text{-P}_2\text{O}_5$. *Solid State Ionics*. 192, 122–125. doi:10.1016/j.ssi.2010.06.018
- Mizuno, F., Hayashi, A., Tadanaga, K., and Tatsumisago, M. (2005). New, highly ion-conductive crystals precipitated from $\text{Li}_2\text{S-P}_2\text{S}_5$ glasses. *Adv. Mater.* 17, 918–921. doi:10.1002/adma.200401286
- Mizuno, F., Hayashi, A., Tadanaga, K., and Tatsumisago, M. (2006). High lithium ion conducting glass-ceramics in the system $\text{Li}_2\text{S-P}_2\text{S}_5$. *Solid State Ionics*. 177, 2721–2725. doi:10.1016/j.ssi.2006.04.017
- Muramatsu, H., Hayashi, A., Ohtomo, T., Hama, S., and Tatsumisago, M. (2011). Structural change of $\text{Li}_2\text{S-P}_2\text{S}_5$ sulfide solid electrolytes in the atmosphere. *Solid State Ionics*. 182, 116–119. doi:10.1016/j.ssi.2010.10.013
- Nagao, M., Hayashi, A., and Tatsumisago, M. (2011). Sulfur-carbon composite electrode for all-solid-state Li/S battery with $\text{Li}_2\text{S-P}_2\text{S}_5$ solid electrolyte. *Electrochim. Acta* 56, 6055–6059. doi:10.1016/j.electacta.2011.04.084
- Nagao, M., Hayashi, A., and Tatsumisago, M. (2012a). Bulk-type lithium metal secondary battery with indium thin layer at interface between Li electrode and $\text{Li}_2\text{S-P}_2\text{S}_5$ solid electrolyte. *Electrochem.* 80, 734–736. doi:10.5796/electrochemistry.80.734
- Nagao, M., Hayashi, A., and Tatsumisago, M. (2012b). High-capacity Li_2S -nanocarbon composite electrode for all-solid-state rechargeable lithium batteries. *J. Mater. Chem* 22, 10015–10020. doi:10.1039/c2jm16802b
- Nagao, M., Hayashi, A., Tatsumisago, M., Ichinose, T., Ozaki, T., Togawa, Y., et al. (2015). Li_2S nanocomposites underlying high-capacity and cycling stability in all-solid-state lithium-sulfur batteries. *J. Power Sources* 274, 471–476. doi:10.1016/j.jpowsour.2014.10.043
- Nagao, M., Hayashi, A., Tatsumisago, M., Kanetsuku, T., Tsuda, T., and Kuwabata, S. (2013). In situ SEM study of a lithium deposition and dissolution mechanism in a bulk-type solid-state cell with a $\text{Li}_2\text{S-P}_2\text{S}_5$ solid electrolyte. *Phys. Chem. Chem. Phys.* 15, 18600–18606. doi:10.1039/c3cp51059j
- Nose, M., Kato, A., Sakuda, A., Hayashi, A., and Tatsumisago, M. (2015). Evaluation of mechanical properties of $\text{Na}_2\text{S-P}_2\text{S}_5$ sulfide glass electrolytes. *J. Mater. Chem. A* 3, 22061–22065. doi:10.1039/C5TA05590C
- Oh, D. Y., Nam, Y. J., Park, K. H., Jung, S. H., Cho, S. J., Kim, Y. K., et al. (2015). Excellent compatibility of solvate ionic liquids with sulfide solid electrolytes: toward favorable ionic contacts in bulk-type all-solid-state lithium-ion batteries. *Adv. Energy Mater.* 5, 1500865. doi:10.1002/aenm.201570120
- Ohtomo, T., Hayashi, A., Tatsumisago, M., and Kawamoto, K. (2013a). Glass electrolytes with high ion conductivity and high chemical stability in the system $\text{LiI-Li}_2\text{O-Li}_2\text{S-P}_2\text{S}_5$. *Electrochemistry* 81, 428–431. doi:10.5796/electrochemistry.81.428
- Ohtomo, T., Hayashi, A., Tatsumisago, M., and Kawamoto, K. (2013b). All-solid-state batteries with $\text{Li}_2\text{O-Li}_2\text{S-P}_2\text{S}_5$ glass electrolytes synthesized by two-step mechanical milling. *J. Solid State Chem.* 17, 2551–2557. doi:10.1007/s10008-013-2149-5
- Ohtomo, T., Hayashi, A., Tatsumisago, M., and Kawamoto, K. (2013c). All-solid-state lithium secondary batteries using the $75\text{Li}_2\text{S-25P}_2\text{S}_5$ glass and the

- 70Li₂S-30P₂S₅ glass-ceramic as solid electrolytes. *J. Power Sources* 233, 231–235. doi:10.1016/j.jpowsour.2013.01.090
- Okita, K., Ikeda, K., Sano, H., Iriyama, Y., and Sakaebe, H. (2011). Stabilizing lithium plating-stripping reaction between a lithium phosphorus oxynitride glass electrolyte and copper thin film by platinum insertion. *J. Power Sources* 196, 2135–2142. doi:10.1016/j.jpowsour.2010.10.014
- Phuc, N., Morikawa, K., Totani, M., Muto, H., and Matsuda, A. (2016). Chemical synthesis of Li₃PS₄ precursor suspension by liquid-phase shaking. *Solid State Ionics*. 285, 2–5. doi:10.1016/j.ssi.2015.11.019
- Sahu, G., Lin, Z., Li, J., Liu, Z., Dudney, N., and Liang, C. (2014). Air-stable, high-conduction solid electrolytes of arsenic-substituted Li₃SnS₄. *Energy Environ. Sci.* 7, 1053–1058. doi:10.1039/C3EE43357A
- Sakuda, A., Hayashi, A., Ohtomo, T., Hama, S., and Tatsumisago, M. (2010). LiCoO₂ electrode particles coated with Li₂S-P₂S₅ solid electrolyte for all-solid-state batteries. *Electrochem. Solid-State Lett.* 13, A73–A75. doi:10.1149/1.3376620
- Sakuda, A., Hayashi, A., Ohtomo, T., Hama, S., and Tatsumisago, M. (2011). All-solid-state lithium secondary batteries using LiCoO₂ particles with pulsed laser deposition coatings of Li₂S-P₂S₅ solid electrolytes. *J. Power Sources* 196, 6735–6741. doi:10.1016/j.jpowsour.2010.10.103
- Sakuda, A., Hayashi, A., Takigawa, Y., Higashi, K., and Tatsumisago, M. (2013a). Evaluation of elastic modulus of Li₂S-P₂S₅ glassy solid electrolyte by ultrasonic sound velocity measurement and compression test. *J. Ceram. Soc. Jpn.* 121, 946–949. doi:10.2109/jcersj2.121.946
- Sakuda, A., Hayashi, A., and Tatsumisago, M. (2013b). Sulfide solid electrolyte with favorable mechanical property for all-solid-state lithium battery. *Sci. Rep.* 3, 2261. doi:10.1038/srep02261
- Sakuda, A., Taguchi, N., Takeuchi, T., Kobayashi, H., Sakaebe, H., Tatsumi, K., et al. (2014). Amorphous niobium sulfides as novel positive-electrode materials. *ECS Electrochem. Lett.* 3, A79–A81. doi:10.1149/2.0091407eel
- Seino, Y., Ota, T., Takada, K., Hayashi, A., and Tatsumisago, M. (2014). A sulfide lithium super ion conductor is superior to liquid ion conductors for use in rechargeable batteries. *Energy Environ. Sci.* 7, 627–631. doi:10.1039/C3EE41655K
- Souquet, J. L., Robinel, E., Barrau, B., and Ribes, M. (1981). Glass formation and ionic conduction in the M₂S-GeS₂ (M=Li, Na, Ag) systems. *Solid State Ionics*. 3-4, 317–321. doi:10.1016/0167-2738(81)90105-3
- Takada, K. (2013). Progress and prospective of solid-state lithium batteries. *Acta Mater.* 61, 759–770. doi:10.1016/j.actamat.2012.10.034
- Tanibata, N., Hayashi, A., and Tatsumisago, M. (2015a). Improvement of rate performance for all-solid-state Na₁₅Sn₄/amorphous TiS₃ cells using 94Na₃PS₄-6Na₄SiS₄ glass-ceramic electrolytes. *J. Electrochem. Soc.* 162, A793–A795. doi:10.1149/2.0011506jes
- Tanibata, N., Matsuyama, T., Hayashi, A., and Tatsumisago, M. (2015b). Improvement of rate performance for all-solid-state Na₁₅Sn₄/amorphous TiS₃ cells using 94Na₃PS₄-6Na₄SiS₄ glass-ceramic electrolytes. *J. Power Sources* 275, 284–287. doi:10.1016/j.jpowsour.2014.10.193
- Tanibata, N., Noi, K., Hayashi, A., Kitamura, N., Idemoto, Y., and Tatsumisago, M. (2014). X-ray crystal structure analysis of sodium-ion conductivity in 94Na₃PS₄-6Na₄SiS₄ glass-ceramic electrolytes. *Chem. Electro. Chem.* 1, 1130–1132. doi:10.1002/celc.201402016
- Tatsumisago, M., and Hayashi, A. (2008). All-solid-state lithium secondary batteries using sulfide-based glass-ceramic electrolytes. *Funct. Mater. Lett.* 1, 31–36. doi:10.1142/S1793604708000071
- Tatsumisago, M., and Hayashi, A. (2014). Sulfide glass-ceramic electrolytes for all-solid-state lithium and sodium batteries. *Int. J. Appl. Glass. Sci.* 5, 226–235. doi:10.1111/ijag.12084
- Tatsumisago, M., Nagao, M., and Hayashi, A. (2013). Recent development of sulfide solid electrolytes and interfacial modification for all-solid-state rechargeable lithium batteries. *J. Asian. Ceram. Soc.* 1, 17–25. doi:10.1016/j.jascer.2013.03.005
- Tatsumisago, M., Shinkuma, Y., and Minami, T. (1991). Stabilization of superionic α -AgI at room temperature in a glass matrix. *Nature* 354, 217–218. doi:10.1038/354217a0
- Teragawa, S., Aso, K., Tadanaga, K., Hayashi, A., and Tatsumisago, M. (2014a). Liquid-phase synthesis of a Li₃PS₄ solid electrolyte using *N*-methylformamide for all-solid-state lithium batteries. *J. Mater. Chem. A* 2, 5095–5099. doi:10.1039/c3ta15090a
- Teragawa, S., Aso, K., Tadanaga, K., Hayashi, A., and Tatsumisago, M. (2014b). Preparation of Li₂S-P₂S₅ solid electrolyte from *N*-methylformamide solution and application for all-solid-state lithium battery. *J. Power Sources* 248, 939–942. doi:10.1016/j.jpowsour.2013.09.117
- Ujiie, S., Hayashi, A., and Tatsumisago, M. (2014). Preparation and electrochemical characterization of (100-x)(0.7Li₂S-0.3P₂S₅)-xLiBr glass-ceramic electrolytes. *Mater. Renew. Sustain. Energy* 3, 1–8. doi:10.1007/s40243-013-0018-x
- Wada, H., Menetrier, M., Levasseur, A., and Hagemuller, P. (1983). Preparation and ionic conductivity of new B₂S₃-Li₂S-LiI glasses. *Mater. Res. Bull.* 18, 189–193. doi:10.1016/0025-5408(83)90080-6
- Yabuchi, N., Kubota, K., Dahbi, M., and Komaba, S. (2015b). Research development on sodium-ion batteries. *Chem. Rev.* 114, 11636–11682. doi:10.1021/cr500192f
- Yamada, A. (2014). Iron-based materials strategies. *MRS Bull.* 39, 423–428. doi:10.1557/mrs.2014.89
- Yamauchi, A., Sakuda, A., Hayashi, A., and Tatsumisago, M. (2013). Preparation and ionic conductivities of (100-x)(0.75Li₂S-0.25P₂S₅)-xLiBH₄ glass electrolytes. *J. Power Sources* 244, 707–710. doi:10.1016/j.jpowsour.2012.12.001
- Yubuchi, S., Hayashi, A., and Tatsumisago, M. (2015a). Sodium-ion conducting Na₃PS₄ electrolyte synthesized via a liquid-phase process using *N*-methylformamide. *Chem. Lett.* 44, 884–886. doi:10.1246/cl.150195
- Yubuchi, S., Teragawa, S., Aso, K., Tadanaga, K., Hayashi, A., and Tatsumisago, M. (2015b). Preparation of high lithium-ion conducting Li₆PS₃Cl solid electrolyte from ethanol solution for all-solid-state lithium batteries. *J. Power Sources* 293, 941–945. doi:10.1016/j.jpowsour.2015.05.093
- Zhang, L., Yang, K., Mi, J., Lu, L., Zhao, L., Wang, L., et al. (2015). Solid electrolytes: Na₃PSe₄: a novel chalcogenide solid electrolyte with high ionic conductivity. *Adv. Energy Mater.* 5, 1501294. doi:10.1002/aenm.201501294
- Zhang, Z., and Kennedy, J. H. (1990). Synthesis and characterization of the B₂S₃-Li₂S, the P₂S₅-Li₂S and the B₂S₃-P₂S₅-Li₂S glass systems. *Solid State Ionics*. 38, 217–224. doi:10.1016/0167-2738(90)90424-P
- Zhu, Z., Chu, I.-H., Deng, Z., and Ong, S. P. (2015). Role of Na⁺ interstitials and dopants in enhancing the Na⁺ conductivity of the cubic Na₃PS₄ superionic conductor. *Chem. Mater.* 27, 8318–8325. doi:10.1021/acs.chemmater.5b03656

Conflict of Interest Statement: The authors declare that the research was conducted in the absence of any commercial or financial relationships that could be construed as a potential conflict of interest.

Copyright © 2016 Hayashi, Sakuda and Tatsumisago. This is an open-access article distributed under the terms of the Creative Commons Attribution License (CC BY). The use, distribution or reproduction in other forums is permitted, provided the original author(s) or licensor are credited and that the original publication in this journal is cited, in accordance with accepted academic practice. No use, distribution or reproduction is permitted which does not comply with these terms.